A Photometric Study of the Contact Binaries CD Sextantis, V365 Sagittae, V1148 Herculis, and NSVS 9027851

Edward J. Michaels
Waffelow Creek Observatory, 10780 FM1878, Nacogdoches, TX 75961; astroed@ejmj.net

Received January 16, 2023; revised February 22, 2023; accepted February 22, 2023

Abstract Multi-band photometric observations were acquired for the eclipsing binary stars CD Sex, V365 Sge, V1148 Her, and NSVS 9027851. These binaries have orbital periods less than 0.37 day, stellar surface temperatures less than solar, and total eclipses at primary minimum. New ephemerides were computed using minima timings from the observations, combined with other timings located in the literature. A period analysis found possible long-term orbital period changes for V1148 Her and V365 Sge. In addition, sinusoidal variations in the O–C residuals of V365 Sge indicate a possible low mass circumbinary companion. Photometric solutions using the Wilson-Devinney (WD) program confirmed that each system is a W-subtype contact binary with fill-outs that range from 15 to 22%. The total eclipses provided reliable solution mass ratios for estimating the absolute parameters of the component stars. All the light curves displayed asymmetries with obvious differences in the brightness of Max I and Max II (O'Connell effect). The asymmetries were attributed to magnetic activity and were modeled as hot and cool spots on the stellar surfaces.

1. Introduction

1.1. Background

Over the past 20 years a number of surveys have identified numerous new contact eclipsing binaries (ASAS, Pojmański 2002; NSVS, Woźniak *et al.* 2004; Hoffman *et al.* 2009; CRTS, Drake *et al.* 2014; ATLAS, Tonry *et al.* 2018). The stars in this study, CD Sex, V365 Sge, V1148 Her, and NSVS 9027851, were classified as W UMa contact binaries in one or more of these surveys. Presented in this paper are new multi-band photometric observations of each star at a higher precision and cadence than provided by the survey data. A brief history of each system is given in the next subsection, with the photometric observations presented in section 2. New minima times, ephemerides, observed properties, and WD light curve analyses are presented in section 3. Discussions of the results are presented in section 4 and conclusions in section 5.

1.2. Notes on individual stars

1.2.1. CD Sex

The variability of CD Sex (GSC 00253-00870, 2MASS J10392274+0135355) was first discovered in the Northern Sky Variability Survey (NSVS; Woźniak *et al.* 2004). Automated variable star classification techniques using NSVS, and All-Sky Automated Survey (ASAS; Pojmański, G. 2002) observations classified it as a W UMa binary (Hoffman *et al.* 2009; Richards *et al.* 2012). The All-Sky Automated Survey for Supernovae (ASAS-SN) catalog also classified the star as a W UMa system with an orbital period of P = 0.2688689 day (Shappee *et al.* 2014; Jayasinghe *et al.* 2018). The Catalina Sky Survey (CRTS) gives a visual magnitude of V = 13.1 with a 0.63-amplitude eclipse (Drake *et al.* 2014). There were six times of minima found in the literature. The Gaia-DR3 parallax gives a distance to this system of d = 288 ± 2 pc (Gaia Collaboration 2022).

1.2.2. V365 Sge

The variability of V365 Sge (GSC 01621-02192, 2MASS J20075538+1731161) was first recognized by Richmond (2002) while observing an outburst of WZ Sge in the same field. He later obtained BVI_c observations of this star and found a maximum visual magnitude of V = 12.5 and a primary eclipse depth of 0.7 magnitude, and classified it as a W UMa contact binary with a period of 0.3690 day. V365 Sge was also given this classification using NSVS observations (Hoffman *et al.* 2009) and from Terrell *et al.*'s (2012) BVR_cI_c photometry. A literature search located eight minima timings for this star. The Gaia-DR3 parallax gives a distance of d = 471 ± 4 pc.

1.2.3. V1148 Her

The variability of V1148 Her (GSC 03494-01097, 2MASS J16012197+4829378) was first reported in the NSVS Skydot catalog (Woźniak *et al.* 2004). An automated classification of NSVS variables identified this star as a W UMa eclipsing binary with an orbital period of P = 0.28229 day (Hoffman *et al.* 2009). The same classification was assigned in the ASAS-SN catalog of variable stars (Jayasinghe *et al.* 2018). A catalog of bright contact binary stars gives a maximum visual magnitude of V = 12.421 and an eclipse amplitude of 0.683 magnitude (Gettel *et al.* 2006). Only two times of minima were located for this star and the Gaia-DR3 parallax gives a distance of d = 288 ± 1 pc.

1.2.4. NSVS 9027851

NSVS 9027851 (2MASS J23231590+3018226, GSC 02752-01272, ASASSN-V J232315.88+301822.9) is located in the constellation Pegasus. It should be noted that a search in the SIMBAD database gives this star's designation as NSVS 6222255, which is not recognized in The International Variable Star Index (VSX; Watson *et al.* 2014). The variability of this star was first discovered in NSVS observations (Woźniak *et al.* 2004). Both the NSVS and ASAS-SN catalogs classified this star as a W UMa eclipsing binary with an orbital period of P = 0.3626625 day, a visual magnitude of V = 13.13, and an eclipse amplitude of 0.57 magnitude (Hoffman *et al.* 2009; Jayasinghe *et al.* 2018). This star has a distance of d = 430 ± 4 pc according to the Gaia-DR3. A literature search did not locate any minima times for this star.

2. Photometric observations

Photometric observations of the close binaries in this study were acquired with a SBIG-STXL CCD camera attached to the 0.36-m Ritchey-Chrétien robotic telescope at the Waffelow Creek Observatory (https://obs.ejmj.net/index.php). The telescope and camera have an image scale of 0.66 arcsec / pixel and a 33.7' × 22.5' field of view. Each star was imaged in four passbands, Johnson V and Sloan g', r', and i'. In addition, V365 Sge and NSVS 9027851 were also imaged in the Johnson B passband. The observation log in Table 1 gives the observation season, the number of nights each star was observed, and the number of images acquired in each passband. The finder charts in Figure 1 show the locations of the comparison and check stars in each field. Table 2 gives the GSC designation, coordinates, and standard magnitudes for all stars used in this study. The standard magnitudes were taken from the AAVSO Photometric All-Sky Survey database (APASS; Henden *et al.* 2015). MIRA software was used for image calibration (bias, dark, and flat correction) and to perform the ensemble aperture photometry of the light images (Mirametrics 2015). The instrumental magnitudes of the variable stars were converted to standard magnitudes. The Heliocentric Julian Date of each observation was converted to orbital phase (φ) using the new linear epochs and orbital periods given in Table 5. Figure 2 shows the folded light curves plotted from orbital phase -0.6 to 0.6, with negative phase defined as φ – 1. The check star magnitudes were plotted below the light curves, which showed no significant variability. The standard error of a single observation ranged from 4 to 10 mmag. The light curve properties are given in Table 3 (Min I, Min II, Max I, Max II, Δm, and total eclipse duration). All the observations can be accessed from the AAVSO International Database (Kafka 2017).

3. Analysis

3.1. Ephemerides

As previously discussed, literature searches located the minima timings available for each star. The primary and secondary minima from the new observations were determined using the Kwee and van Woerden (1956) method. Several additional minima times were derived using observations with sufficient nightly cadence from the AAVSO and SuperWASP databases. All the minima times and errors are compiled in Table 4. This table also shows the cycle numbers and the difference between the observed and predicted minima times (O–C). The predicted minima times were calculated using the reference epochs and orbital periods given in Table 5. New linear light elements were computed by least-squares solution using the O–C residuals. The regression results and residuals are shown in the O–C diagrams in Figure 3 and the new linear light elements in Table 5.

The residuals from the regression analysis of V365 Sge indicate the orbital period of this binary may be undergoing a long-term linear and possibly a cyclic period change (see Figure 3). A long-term period change reveals itself as a parabolic trend in the O–C residuals and a cyclic change as a sinusoidal trend. A long-term period change is frequently attributed to mass transfer between the component stars or loss of angular momentum from the system. An apparent cyclic period change can result from a light-time effect (LITE) caused by a circumbinary companion. It is not uncommon for contact binaries to have a third star orbiting around them (Liao and Qian 2010; Qian *et al.* 2013; Pribulla and Ruciński 2006). The sinusoidal variation in the residuals appears symmetrical, which indicates a circular orbit for a tertiary component (see bottom panel in Figure 4). To describe the general trend of the O–C residuals, the following equation was used to investigate the parabolic and sinusoidal variations in the orbital period:

$$\text{HJD Min I} = \text{HJD}_0 + \text{PE} + \text{QE}^2 + \text{A} \sin(\omega\text{E} + \varphi). \quad (1)$$

The first three terms ($\text{HJD}_0 + \text{PE} + \text{QE}^2$) is the quadratic ephemeris where Q measures the long-term period change, and the fourth term is the time difference resulting from the orbital motion of the binary about the barycenter of a tertiary system. For the regression analysis the following weights were assigned to individual minima times: w = 1 for times derived from visual observations and w = 10 for CCD observations. The parameter values HJD_0, P, Q, A, ω, and φ were determined using the Levenberg-Marquardt algorithm, which gives the following ephemeris:

$$\begin{aligned}\text{HJD Min I} = {} & 2459767.6180(1) + 0.3691265(5)\,\text{E} \\ & -2.889(2) \times 10^{-10}\,\text{E}^2 \\ & + 0.001887(2) \sin(0.0005278(4)\,\text{E} + 0.494(5)). \end{aligned} \quad (2)$$

The negative quadratic coefficient in Equation 2 suggests a slowly decreasing orbital period with a rate of $-1.055(2) \times 10^{-7}$ d · yr^{-1}, or about 1 second per century. The top panel of Figure 4 shows the O–C diagram where the solid line represents Equation 2, a combination of the long-term period change and the cyclic LITE variation caused by the proposed tertiary component. The dashed line is the quadratic component in this equation. The middle panel shows the residuals after removing the downward parabolic change and the cyclic variation. In the bottom panel only the quadratic term of Equation 2 is subtracted to show the periodic variation more clearly. The results of this period analysis will be discussed further in section 5.

The residuals from the linear regression analysis of V1148 Her also has a parabolic shape which indicates a possible long-term linear period change (see Figure 3). A second least-squares solution of the O–C residuals in Table 4 gives the following quadratic ephemeris:

$$\begin{aligned}\text{HJD Min I} = {} & 2459771.794(3) + 0.2822539(1)\,\text{E} \\ & + 1.28(3) \times 10^{-11}\,\text{E}^2. \end{aligned} \quad (3)$$

The positive sign of the quadratic coefficient indicates the period is increasing at a rate of $\text{dP/dt} = 3.31(9) \times 10^{-8}$ d·yr^{-1}. This slow period change should be considered preliminary since it was determined from a relatively small number of minima timings. The dashed line in the O–C diagram of Figure 5 (top panel) represents Equation 3 with the residuals in the bottom panel.

Table 1. Observation Log.

System	Dates	No. Nights	Images Acquired				
			B	*V*	*g′*	*r′*	*i′*
CD Sex	2022 Mar	13	--	457	711	620	625
V365 Sge	2020 Aug	24	771	665	531	523	510
V1148 Her	2020 Jun/Jul	14	--	1375	637	701	448
NSVS 9027851	2022 Sep	13	747	861	685	729	881

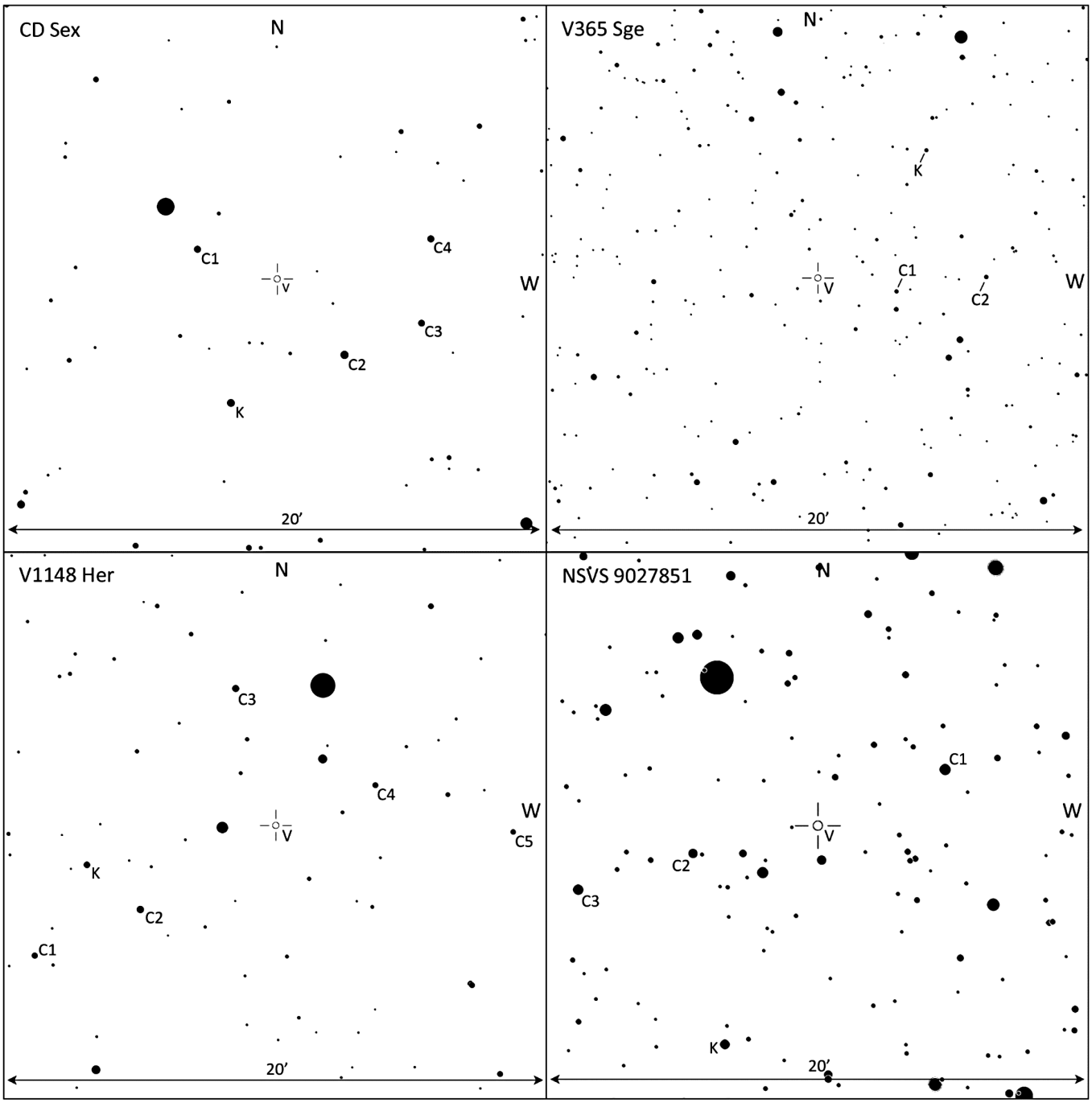

Figure 1. Finder charts showing the locations of the binary (V), comparison (C1–C6), and check (K) stars for each system. The comparison star designations correspond to the values in Table 2.

Table 2. APASS (Henden *et al.* 2015) Comparison and Check Star Magnitudes.

System	*R.A. (2000)* *h*	*Dec. (2000)* °	*B*	*V*	*g′*	*r′*	*i′*
CD Sex	10.65631	+1.59310					
GSC 00253-00725 (C1)	10.65950	+1.61099	—	12.735	12.966	12.590	12.460
GSC 00253-00688 (C2)	10.65361	+1.54740	—	12.286	12.611	12.057	11.849
GSC 00253-01037 (C3)	10.65053	+1.56658	—	12.831	13.045	12.717	12.585
GSC 00253-00243 (C4)	10.65016	+1.61724	—	12.702	12.903	12.599	12.494
GSC 00253-00964 (K)	10.65816	+1.51859	—	12.427	12.587	12.340	12.255
Standard deviation of observed K-star magnitudes			—	± 0.004	± 0.004	± 0.004	± 0.006
V365 Sge	20.13205	+17.52113					
GSC 01621-02177 (C1)	20.12876	+17.51321	13.901	12.820	13.253	12.396	11.826
GSC 01621-02205 (C2)	20.12499	+17.52172	12.764	12.472	12.511	12.361	12.244
GSC 01621-01948 (K)	20.12750	+17.59833	14.094	13.131	13.506	12.777	12.358
Standard deviation of observed K-star magnitudes			± 0.015	± 0.008	± 0.010	± 0.006	± 0.008
V1148 Her	16.02276	+48.49413					
GSC 03494-01301 (C1)	16.03723	+48.41505	—	13.289	13.478	13.149	13.000
GSC 03494-00204 (C2)	16.03090	+48.44308	—	12.848	13.312	12.501	12.202
GSC 03494-00893 (C3)	16.02518	+48.57641	—	12.862	13.227	12.580	12.291
GSC 03494-00980 (C4)	16.01677	+48.51808	—	13.399	13.670	13.213	13.025
GSC 03494-00963 (C5)	16.00849	+48.48968	—	13.674	13.995	13.460	13.235
GSC 03494-00516 (K)	16.03412	+48.46998	—	13.096	13.302	12.940	12.770
Standard deviation of observed K-star magnitudes			—	± 0.010	± 0.007	± 0.007	± 0.008
NSVS 9027851	23.38775	+30.30626					
GSC 02752-01546 (C1)	23.38169	+30.34064	13.224	12.455	12.792	12.226	11.992
GSC 02752-01892 (C2)	23.39369	+30.28903	13.879	13.099	13.441	12.841	12.591
GSC 02752-01924 (C3)	23.39915	+30.26692	13.680	12.846	13.214	12.588	12.318
GSC 02752-01240 (K)	23.39217	+30.17197	13.857	13.023	13.388	12.743	12.461
Standard deviation of observed K-star magnitudes			± 0.012	± 0.006	± 0.006	± 0.005	± 0.006

Table 3. Light curve properties.

	Min I Mag.	*Min II Mag.*	*Max I Mag.*	*Max II Mag.*	*Delta Mag. Max II - Min I*	*Total Eclipse Duration (minutes)*
CD Sex						
V	13.943 ± 0.014	13.850 ± 0.007	13.153 ± 0.005	13.127 ± 0.010	0.816 ± 0.008	≈ 12
g'	14.365 ± 0.013	14.279 ± 0.013	13.563 ± 0.011	13.526 ± 0.005	0.839 ± 0.027	≈ 12
r'	13.610 ± 0.009	13.522 ± 0.003	12.860 ± 0.004	12.820 ± 0.006	0.791 ± 0.002	≈ 12
i'	13.278 ± 0.013	13.200 ± 0.014	12.546 ± 0.008	12.525 ± 0.008	0.753 ± 0.012	≈ 11
V365 Sge						
B	14.042 ± 0.010	13.906 ± 0.012	13.253 ± 0.007	13.263 ± 0.004	0.779 ± 0.011	≈ 27
V	13.381 ± 0.006	13.283 ± 0.010	12.652 ± 0.007	12.680 ± 0.007	0.701 ± 0.017	≈ 27
g'	13.597 ± 0.019	13.485 ± 0.012	12.844 ± 0.005	12.866 ± 0.006	0.732 ± 0.056	≈ 27
r'	13.119 ± 0.012	13.014 ± 0.004	12.411 ± 0.004	12.432 ± 0.007	0.688 ± 0.038	≈ 27
i'	12.795 ± 0.007	12.702 ± 0.007	12.122 ± 0.001	12.137 ± 0.005	0.658 ± 0.049	≈ 27
V1148 Her						
V	13.135 ± 0.012	13.086 ± 0.013	12.465 ± 0.006	12.526 ± 0.005	0.609 ± 0.008	≈ 20
g'	13.427 ± 0.008	13.380 ± 0.010	12.745 ± 0.006	12.818 ± 0.009	0.610 ± 0.046	≈ 20
r'	12.910 ± 0.003	12.859 ± 0.003	12.262 ± 0.003	12.318 ± 0.003	0.593 ± 0.004	≈ 21
i'	12.648 ± 0.008	12.605 ± 0.007	12.024 ± 0.005	12.072 ± 0.002	0.576 ± 0.011	≈ 20
NSVS 9027851						
B	14.410 ± 0.014	14.352 ± 0.013	13.758 ± 0.017	13.818 ± 0.009	0.592 ± 0.017	≈ 32
V	13.527 ± 0.005	13.477 ± 0.010	12.916 ± 0.006	12.963 ± 0.007	0.564 ± 0.023	≈ 31
g'	13.926 ± 0.011	13.862 ± 0.004	13.295 ± 0.005	13.334 ± 0.007	0.592 ± 0.030	≈ 31
r'	13.244 ± 0.003	13.200 ± 0.008	12.657 ± 0.004	12.683 ± 0.005	0.561 ± 0.037	≈ 31
i'	12.956 ± 0.009	12.907 ± 0.007	12.381 ± 0.004	12.413 ± 0.006	0.543 ± 0.010	≈ 30

Table 4. Times of minima and O–C residuals.

Epoch HJD 2400000+	*Error*	*Cycle*	*O–C*	*Ref.*
CD Sex				
55259.9227	0.00010	0.0	0.00000	5
55591.8422	0.00020	1234.5	–0.00052	6
55591.9765	0.00010	1235.0	–0.00065	6
55671.6958	0.00080	1531.5	–0.00130	6
55959.9224	0.00050	2603.5	–0.00334	8
56015.7154	0.00020	2811.0	–0.00087	8
57530.7919	—	8446.0	–0.00678	2
59638.7252	0.00007	16286.0	–0.01436	19
59638.8592	0.00006	16286.5	–0.01476	19
59648.8072	0.00010	16323.5	–0.01499	19
59649.6135	0.00009	16326.5	–0.01526	19
59650.8240	0.00011	16331.0	–0.01462	19
59669.6453	0.00012	16401.0	–0.01426	19
59669.7785	0.00012	16401.5	–0.01554	19
59670.7205	0.00012	16405.0	–0.01451	19
V365 Sge				
[a] 52122.660	0.002	0.0	0.00000	17
[a] 52526.304	0.005	1093.5	0.00089	3
[a] 52526.486	0.003	1094.0	–0.00167	3
[a] 52530.363	0.004	1104.5	–0.00053	3
[a] 52533.496	0.003	1113.0	–0.00513	3
[a] 52574.298	0.006	1223.5	0.00806	3
[a] 52576.322	0.004	1229.0	0.00184	3
[a] 52708.658	0.003	1587.5	0.00492	3
[a] 52764.582	0.003	1739.0	0.00580	3
[a] 52791.525	0.006	1812.0	0.00235	3
[a] 52813.489	0.004	1871.5	0.00314	3
[a] 52814.411	0.004	1874.0	0.00232	3
[a] 52829.536	0.003	1915.0	–0.00699	4
[a] 52839.512	0.004	1942.0	0.00251	4
[a] 52877.532	0.005	2045.0	0.00217	4
[a] 52886.393	0.004	2069.0	0.00406	4
[a] 52903.364	0.004	2115.0	–0.00489	4
[a] 52945.261	0.003	2228.5	–0.00409	4
[a] 52967.232	0.003	2288.0	0.00370	4
[a] 53003.224	0.004	2385.5	0.00558	4
[a] 53094.578	0.003	2633.0	0.00003	4
[a] 53121.532	0.004	2706.0	0.00757	4
[a] 53214.545	0.006	2958.0	–0.00006	18
[a] 53233.366	0.004	3009.0	–0.00467	18
[a] 53257.355	0.002	3074.0	–0.00908	18
[a] 53267.319	0.002	3101.0	–0.01158	18
55028.4226	0.0004	7872.0	–0.02482	14
55067.3656	0.0014	7977.5	–0.02499	14
55352.5146	0.0009	8750.0	–0.02853	13
55362.8485	0.0002	8778.0	–0.03025	5
55389.4280	0.0011	8850.0	–0.02808	9
55828.6892	0.0006	10040.0	–0.03098	7
56094.4591	0.0012	10760.0	–0.03432	12
56539.4421	0.0016	11965.5	–0.03693	11
[b] 57254.6208	0.0002	13903.0	–0.04663	1
[b] 57262.5553	0.0005	13924.5	–0.04846	1
[b] 57976.8135	0.0001	15859.5	–0.05577	1
[b] 57977.9204	0.0001	15862.5	–0.05626	1
[b] 57980.8738	0.0001	15870.5	–0.05588	1
[b] 57981.7959	0.0001	15873.0	–0.05665	1
[b] 57992.8697	0.0001	15903.0	–0.05669	1
[b] 58002.8360	0.0001	15930.0	–0.05692	1
59068.6818	0.0002	18817.5	–0.07252	19
59068.8653	0.0001	18818.0	–0.07364	19
59069.7889	0.0002	18820.5	–0.07284	19
59070.7109	0.0002	18823.0	–0.07368	19
59072.7422	0.0001	18828.5	–0.07261	19
59073.6639	0.0001	18831.0	–0.07370	19
59073.8495	0.0001	18831.5	–0.07267	19
59074.7712	0.00022	18834.0	–0.07381	19
59075.6951	0.00027	18836.5	–0.07274	19
59076.8025	0.00010	18839.5	–0.07273	19
59077.7242	0.00009	18842.0	–0.07387	19
59080.6773	0.00009	18850.0	–0.07380	19
59082.7087	0.00011	18855.5	–0.07264	19
59767.8015	0.00008	20711.5	–0.08411	19
V1148 Her				
51399.8490	—	0.0	0.00000	15
[c] 54297.4693	0.0001	10266.0	–0.00955	16
57100.5368	0.0006	20197.0	–0.01643	10
[b] 58999.8269	0.0001	26926.0	–0.02028	1
59012.8109	0.0001	26972.0	–0.01995	19
59013.6578	0.0000	26975.0	–0.01986	19
59014.7869	0.0001	26979.0	–0.01976	19
59016.7628	0.0001	26986.0	–0.01966	19
59020.7143	0.0001	27000.0	–0.01974	19
59021.8435	0.0001	27004.0	–0.01951	19
59771.6531	0.0001	29660.5	–0.02036	19
59771.7939	0.0001	29661.0	–0.02062	19
NSVS 9027851				
[c] 53180.6946	0.0007	0.0	0.00000	16
[c] 53184.6853	0.0006	11.0	0.00136	16
[c] 53192.6637	0.0008	33.0	0.00122	16
[c] 53196.6534	0.0025	44.0	0.00161	16
[c] 53200.6437	0.0025	55.0	0.00259	16
[c] 53204.6315	0.0028	66.0	0.00113	16
[c] 53220.5873	0.0031	110.0	–0.00019	16
[c] 53240.5364	0.0030	165.0	0.00243	16
[c] 53252.5020	0.0025	198.0	0.00016	16
[c] 53270.6353	0.0034	248.0	0.00034	16
[c] 53938.6604	0.0020	2090.0	0.00115	16
[c] 53942.6472	0.0023	2101.0	–0.00134	16
[c] 53950.6283	0.0026	2123.0	0.00116	16
[c] 53970.5737	0.0031	2178.0	0.00010	16
[c] 54001.3994	0.0024	2263.0	–0.00050	16
[c] 54022.4339	0.0030	2321.0	–0.00038	16
[c] 54050.3609	0.0020	2398.0	0.00158	16
59839.8957	0.0001	18362.0	–0.00776	19
59841.7085	0.0001	18367.0	–0.00824	19
59846.7853	0.0001	18381.0	–0.00873	19
59848.5989	0.0002	18386.0	–0.00843	19
59849.6867	0.0002	18389.0	–0.00863	19

(a) Visual Minima (all other minima in this table were derived from CCD observations).
(b) Minima derived from AAVSO data.
(c) Minima derived from SuperWASP data.

References: (1) AAVSO (Kafka 2017); (2) ASAS-SN (Shappee, et al. *2014; Jayasinghe,* et al. *2019); (3) Diethelm (2003); (4) Diethelm (2004); (5) Diethelm (2010); (6) Diethelm (2011); (7) Diethelm (2012a); (8) Diethelm (2012b); (9) Hübscher (2011); (10) Hübscher (2016); (11) Hübscher (2014); (12) Hübscher and Lehmann (2013); (13) Hübscher and Monninger (2011); (14) Hübscher* et al. *(2010); (15) Khruslov (2006); (16) SuperWASP (Masaryk Univ. 2022); (17) Richmond (2002); (18) Locher (2005); (19) this paper.*

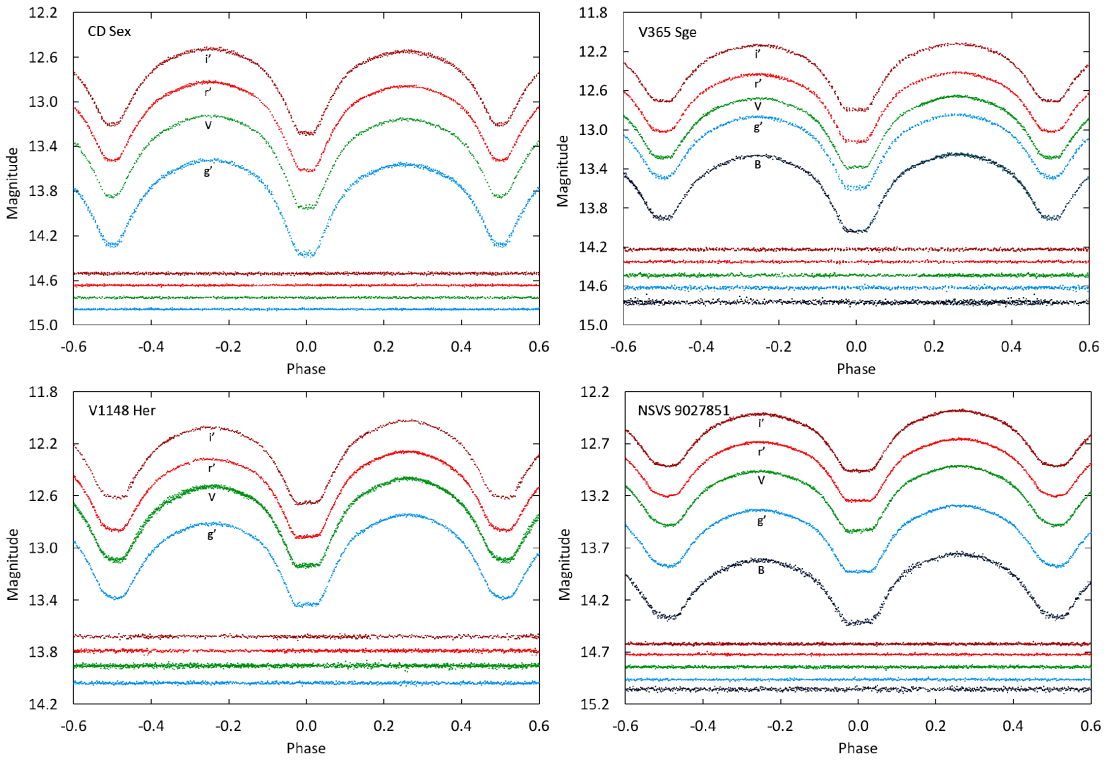

Figure 2. The folded light curves in standard magnitudes. From top to bottom the passbands are i', r', V, and g' for the stars CD Sex and V1148 Her, and i', r', V, g', and B for V365 Sge and NSVS 9027851. The bottom curves in each panel are the offset check star magnitudes in the same passband order as the light curves. Error bars were omitted from the plotted points for clarity.

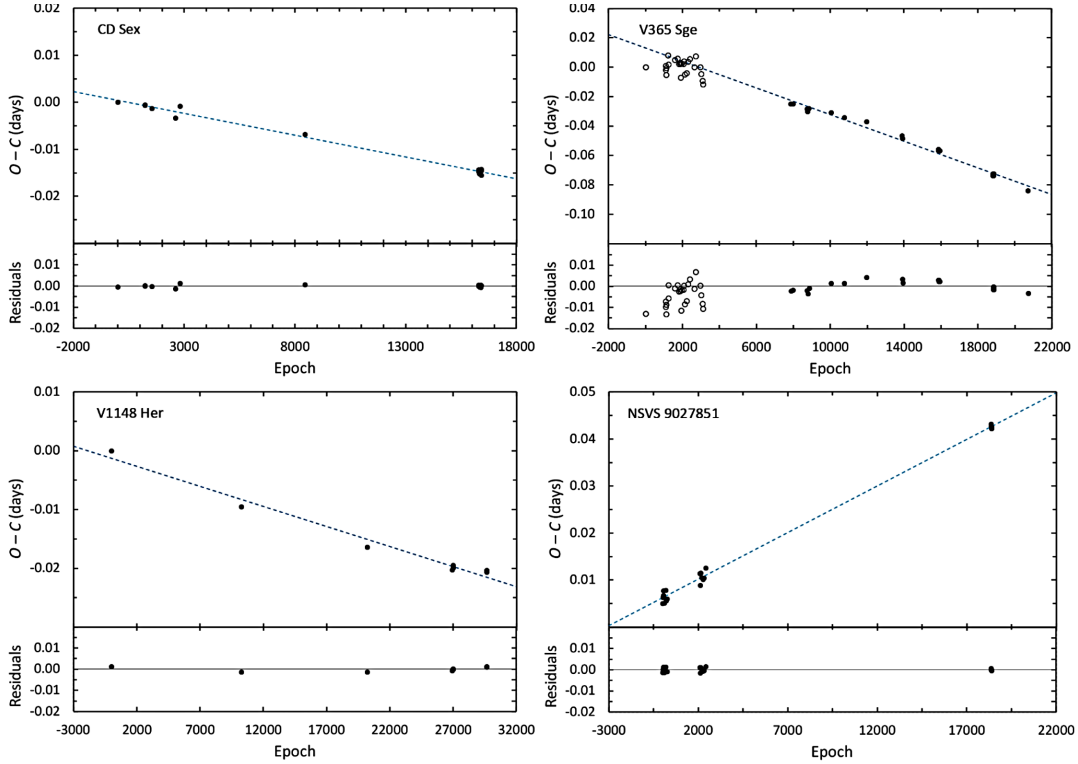

Figure 3. The top panel shows the O–C residuals that were calculated from the reference ephemeris for each star (see Table 5). The open circles are visually determined minima and the filled circles CCD minima. The dashed lines are the linear fits to the residuals. The bottom panel of each diagram shows the residuals from each fit.

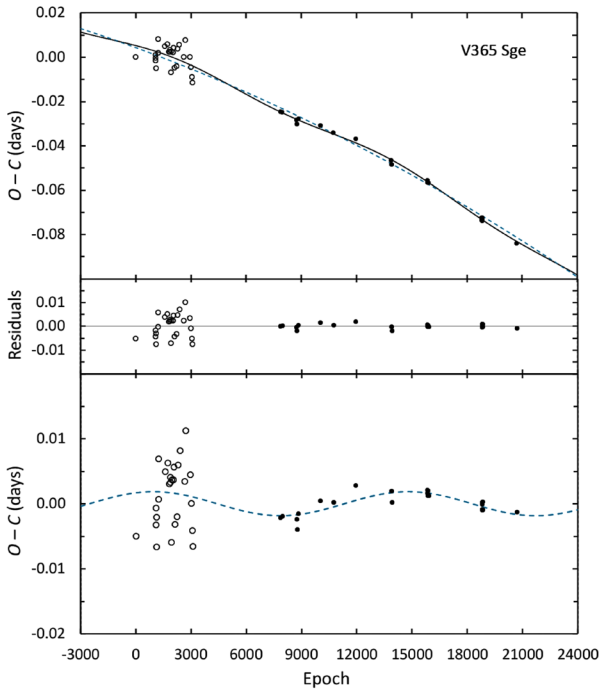

Figure 4. The top panel shows the O–C residuals that were calculated from the reference ephemeris for V365 Sge (see Table 5). The open circles are the visually determined minima and the filled circles the CCD minima. The solid line corresponds to Equation 2, which shows the fit for a circular orbit (e = 0) of a supposed third body. The dashed line refers to the quadratic term in this equation. The middle panel shows the residuals after removing the downward parabolic change and the cyclic variation. In the bottom panel the quadratic term of Equation 2 is subtracted to show the periodic variation more clearly.

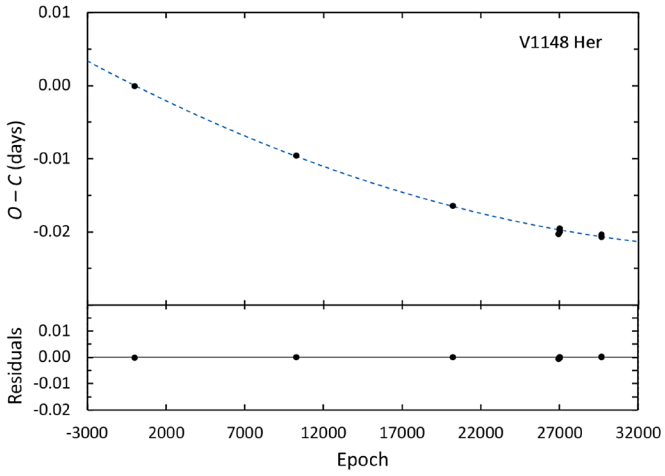

Figure 5. The O–C residuals (filled-circles) were calculated from the reference ephemeris for V1148 Her (see Table 5). The dashed line is the quadratic fit to the residuals. The bottom panel shows the residuals after removing the upward parabolic change.

3.2. Color, temperature, spectral type, absolute magnitude, luminosity

The averaged observed color of each system was determined by binning the phase and magnitude of the B and V observations with a phase width of 0.01. The phases and magnitudes in each bin interval were averaged. The binned V magnitudes were subtracted from the linearly interpolated B magnitudes, resulting in an observed (B–V) color at each phase point. Since B observations were not available for CD Sex and V1148 Her, the binning process used the g' and r' observations to give the (g'– r') colors for these two stars. The (g'– r') colors were converted to (B–V) colors using the transformation equation of Jester et. al (2005):

$$(B–V) = 0.98(g' – r') + 0.22. \quad (4)$$

The observed colors were corrected using color excess values from three-dimensional dust maps based on Pan-STARRS 1 and 2MASS photometry and Gaia parallaxes (Green *et al.* 2019). The V passband apparent magnitudes were corrected for interstellar extinction (A_V), using the extinction to reddening ratio of $A_V / E(B–V) = 3.1$. The absolute visual magnitude (M_V) of each star was computed using the following equation:

$$M_V = V – A_V – 5 \log (d / 10), \quad (5)$$

where V is the apparent magnitude at the brightest quadrature (see Table 3), A_V is the extinction, and d the Gias-DR3 distance in parsecs (Gaia Collaboration 2022). The visual luminosity of each system in solar units was calculated from the following equation:

$$M_V = M_{V\odot} – 2.5 \log (L / L_\odot), \quad (6)$$

Where $M_{V\odot} = 4.81$ is the absolute visual magnitude of the sun (Willmer 2018). The effective temperatures were computed using the corrected colors in the empirically derived equation of Eker *et al.* (2020):

$$\log T_{eff} = 0.07569(0.012) \times (B–V)_0^2 \\ –0.38786(0.01368) \times (B–V)_0 + 3.96617(0.00338). \quad (7)$$

For each binary, the color excess, visual extinction, the average dereddened color, Gaia-DR3 distance, extinction-corrected visual magnitude, absolute visual magnitude, and visual luminosity are shown in Table 6. Compiled in Table 7 are the effective temperatures derived from the corrected color and the estimated spectral type of each system. For comparison with the color derived temperatures, this table also contains values collected from three surveys using the VizieR Online Data Catalog—LAMOST, Gaia-DR3, and 2MASS. The temperatures from these surveys compared reasonably well with dereddened color temperatures having differences of less than 300 K. The one outlier was the 2MASS temperature for V365 Sge; it was 479 K greater than the color derived temperature.

3.3. Light curve modeling

W UMa-type contact binaries are characterized by continuous brightness variations and nearly equal light curve minima, as is certainly the case for the stars in this study. In addition, the light curves of each system reveal total eclipses at their deepest minima ($\varphi = 0$) and asymmetries likely resulting from spotting caused by their magnetically active dwarf stars. This light curve morphology indicates these systems are W-subtype contact binaries with the larger and cooler primary star eclipsing the hotter secondary star at primary minima. Given that each system displays a total primary eclipse, photometric light curve solutions should provide for well-determined mass ratios, $q = m_2 / m_1$, where the subscripts 1 and 2 refer to the more massive primary star and the less massive secondary component, respectively (Wilson 1978; Terrell and Wilson 2005; Hambálek and Pribulla 2013).

Photometric light curve solutions for each binary were obtained using the 2015 version of the Wilson-Devinney (WD) program (Wilson and Devinney 1971; van Hamme and Wilson 1998). The simultaneous solutions utilized four passbands, Johnson V and Sloan g', r', and i'. The input data for each color consisted of 100 binned points formed from the observed standard magnitudes (see section 3.2). These points were converted to normalized flux, with each point weighted by the number of observations forming that point. The WD program was configured for overcontact binaries (Mode 3), the Kurucz (2002) stellar atmosphere model was applied, and the logarithmic limb darkening coefficients were calculated by the method of van Hamme (1993). For CD Sex, V1148 Her, and NSVS 9027851, the effective temperature (T_1) of the primary star was fixed at the LAMOST values in Table 7. Since a spectroscopically-determined temperature was not available for V365 Sge, its effective temperature was fixed at the value determined from the observed color corrected for reddening. All the stellar effective temperatures were well below 7200 K; therefore, standard convective parameters for gravity brightening and bolometric albedo were fixed at $g_1 = g_2 = 0.32$ and $A_1 = A_2 = 0.5$, respectively (Lucy 1968; Ruciński 1969). The adjustable parameters include the inclination (i), mass ratio ($q = m_2 / m_1$), potential ($\Omega_1 = \Omega_2$), temperature of the secondary star (T_2), the band-specific luminosity for each wavelength (L), and third light (l_3). To address the light curve asymmetries, star spots were included in each system's model. The following parameters were adjustable for each spot modeled: colatitude, longitude, spot radius, and temperature factor (T_{spot} / T_{eff}). Before attempting WD solution iterations, a preliminary fit to the light curves was made using the BINARY MAKER 3.0 program (BM3; Bradstreet and Steelman 2002). The parameters resulting from the BM3 model fits were used as the inputs for the WD simultaneous four-color light curve solutions. The Method of Multiple Subsets (MMS; Wilson and Biermann 1976) was employed to minimize strong correlations of the parameters. Throughout the solution iteration process, the third-light corrections for each system were negligibly small (or negative). This indicates that if any stellar third-bodies are orbiting the binaries or if there are unresolved field stars, the contribution of these sources to the total system light is small. The final best-fit solution parameters for each system are shown in Table 8. The filling-factors were computed using the method of Lucy and Wilson (1979):

$$f = (\Omega_{inner} - \Omega) / (\Omega_{inner} - \Omega_{outer}), \quad (8)$$

where Ω_{inner} and Ω_{outer} are the inner and outer critical equipotential surfaces and Ω is the equipotential that describes the common envelope stellar surface. Figures 6 and 7 display the normalized light curves overlaid by the synthetic solution curves (solid lines) with the residuals shown in the bottom panels. A BM3 graphical representation of each system solution is shown in Figure 8 (Bradstreet and Steelman 2002).

4. Discussion

The light curve solutions confirmed that each system belongs to the W-type subclass of W UMa systems, where the less massive hotter component is eclipsed at primary minimum. The high inclinations ($i > 86°$) and the smaller secondary stars resulted in total eclipses at primary minimum. Each system is in an overcontact configuration but not excessively so with the degree of fill-out ranging from 15 to 23%. A large majority of totally eclipsing W UMa systems with well determined parameters have mass ratios that range from 0.1 to 0.5 (Latković and Lazarević 2021). The mass ratios of the stars in this study fall within that range, 0.33–0.50. The primary stars were all cooler than the sun, with spectral types from K3 to G7. The temperature differences between the component stars ($\Delta T = T_2 - T_1$) ranged from 233 K for CD Sex to 381K for V365 Sge. During modeling, hot or cool spots were necessary to fit the light curve asymmetries. This stellar dynamo magnetic activity was not unexpected, given the convective envelopes and rapid rotation of the stars. It should be noted that the solution spot parameters are not definitive; other spot configurations may give equal or better results (Terrell 2022).

Radial velocity observations were not available for the stars in this study, but provisional absolute stellar parameters can be calculated with the binary's mass ratio and an estimate of the primary star's mass. The photometric solutions provided the mass ratios and the primary stars' masses were calculated using Latković *et al*'s (2021) period-mass relation for W UMa binaries:

$$M_1 = (2.94 \pm 0.21) P + (0.16 \pm 0.08). \quad (9)$$

The secondary star masses (M_2) were computed from the solution mass ratio. The distance between the mass centers of the two stars was calculated using Kepler's Third Law. Using this distance as an input parameter, the volume radii were calculated by the WD light curve program (LC). The bolometric magnitudes of each star were calculated using the following equation:

$$M_{bol} = -10 \log (T / T_\odot) - 5 \log (R / R_\odot) + M_{bol,\odot}, \quad (10)$$

and the luminosities in solar units using the Stefan-Boltzmann law:

Table 5. Ephemeris elements for HJD Min I.

System	Reference Elements Epoch 2400000+	P_{orb} (days)	New Linear Elements Epoch 2400000+	P_{orb} (days)
CD Sex	155259.9227	10.268870	59670.7203 (1)	0.26886907 (1)
V365 Sge	255028.4226	30.3691295	59767.6202 (4)	0.36912494 (2)
V1148 Her	451399.849	40.282255	59771.793 (1)	0.2822543 (1)
NSVS 9027851	553180.695	60.36266	59849.687 (1)	0.362662 (1)

References: (1) Diethelm 2010; (2) Hübscher 2010; (3) ASAS-SN (Shappee, et al. *2014; Jayasinghe,* et al. *2019); (4) Khruslov 2006; (5) SuperWASP (Masaryk Univ. 2022); (6) Watson* et al. *2014.*

Table 6. Color excess, visual extinction, dereddened color, Gaia-DR3 distance, extinction corrected apparent visual magnitude at quadrature, calculated absolute visual magnitude and visual luminosity.

	CD Sex	V365 Sge	V1148 Her	NSVS 9027851
E(B–V)	0.021 ± 0.016	0.018 ± 0.016	0.027 ± 0.008	0.150 ± 0.009
A_V	0.066 ± 0.013	0.055 ± 0.095	0.082 ± 0.023	0.464 ± 0.027
$(B–V)_0$	0.903 ± 0.013	0.643 ± 0.020	0.682 ± 0.013	0.711 ± 0.014
Dist. (pc)	288 ± 2	471 ± 4	288 ± 1	430 ± 4
V	13.06 ± 0.02	12.60 ± 0.10	12.38 ± 0.02	12.45 ± 0.03
M_V	5.76 ± 0.02	4.23 ± 0.10	5.08 ± 0.03	4.28 ± 0.03
$L_{V\odot}$	0.42 ± 0.01	1.70 ± 0.15	0.78 ± 0.02	1.63 ± 0.05

Table 7. Effective temperatures from dereddened $(B–V)_0$ colors compared with other surveys and approximate spectral class.

System	$(B-V)_0$ $T_{eff}(K)$	LAMOST $T_{eff}(K)$	Gaia-DR3 $T_{eff}(K)$	2Mass $T_{eff}(K)$	Spectral Class
CD Sex	4762 ± 267	4865 ± 64	5088 ± 8	4948 ± 160	K2–K3
V365 Sge	5598 ± 261	—	5855 ± 12	6077 ± 175	F9–G7
V1148 Her	5457 ± 202	5161 ± 64	5437 ± 10	5391 ± 139	K1–G8
NSVS 9027851	5352 ± 209	5533 ± 88	5620 ± 26	5515 ± 149	G9–G6

$$L / L_\odot = (R / R_\odot)^2 (T / T_\odot)^4. \quad (11)$$

Compiled in Table 9 are the estimated absolute stellar parameters: the masses (M_1, M_2), distance between the mass centers (a), volume radii (R_1, R_2), bolometric magnitudes ($M_{bol,1}$, $M_{bol,2}$), luminosities (L_1, L_2), and surface gravities (g_1, g_2).

The distance modulus ($V – M_V$) was used to estimate the distance to each system. The apparent magnitude V in this estimation utilized the observed magnitude at the brightest quadrature (corrected for extinction). The system absolute magnitudes (M_V) were computed using the bolometric magnitudes and the bolometric corrections for each star. The bolometric corrections were interpolated from the tables of Pecaut and Mamajek (2013) according to the effective temperatures of the component stars. By combining the visual luminosities of the component stars, the system absolute magnitude M_V was derived for each binary. The estimated distances of each system could then be compared to the Gaia-DR3 distances (see section 5).

The period analysis of V365 Sge revealed a possible circumbinary companion. The orbital period of the proposed third body was computed using the relation $P_3 = 2\pi P/\omega$, where $\omega = 5.278(4) \times 10^{-4}$ is the angular frequency from Equation 2 and P is the orbital period of V365 Sge. This gives an estimated period of $P_3 = 12.032 \pm 0.009$ yr of the tertiary companion. Assuming a circular orbit ($e = 0$), the projected orbital radius of the binary about the barycenter was calculated from this relation, $a_{12} \sin i_3 = A_3 \times c$, where Equation 2 gives the amplitude of the cyclic variation, $A_3 = 1.887(3) \times 10^{-3}$ days, and c is the speed of light. For a coplanar orbit with the binary, the mass and orbital radius of the third body were computed using the mass function and the provisional masses of the binary components (see Table 9). The mass function was determined using the following well-known equation:

$$f(m) = \frac{4\pi 2}{GP_3^2} (a_{12} \sin l_3) = \frac{(M_3 \sin l_3)^3}{(M_1 + M_2 + M_3)^2}. \quad (12)$$

where G is the gravitational constant. The third body's mass, calculated by the iteration method and its orbital radius using Kepler's Third Law, gives the following values: $M_3 = 0.094 \pm 0.004\, M_\odot$ and $a_3 = 6.1 \pm 0.1$ AU. This low mass suggests a very dim red dwarf star with a luminosity of 0.0007 $L_\odot$ (Pecaut and Mamajek 2013). The contribution to the total system light would only amount to about 0.0003%, which would not have produced a noticeable third light (l_3) in the WD solution. Table 10 gives the tertiary component parameters, including computed masses and orbital radii for inclinations of 30°, 60°, and 90°. The presence of a third star in this system was based upon the sinusoidal component of the O–C residuals, which only covers about one orbital cycle.

Table 8. Results derived from light curve modeling.

Parameter	*CD Sex*	*V365 Sge*	*V1148 Her*	*NSVS 9027851*
Filling factor	15%	20%	20%	22%
i (°)	87.7 ± 0.8	89.1 ± 0.5	88 ± 1	86.7 ± 0.7
T_1 (K)	[1]4865	15598	15161	15533
T_2 (K)	5098 ± 3	5980 ± 8	5403 ± 6	15779 ± 7
$\Omega_1 = \Omega_2$	2.836 ± 0.010	2.657 ± 0.004	2.570 ± 0.006	2.483 ± 0.007
$q(m_2 / m_1)$	0.502 ± 0.006	0.415 ± 0.003	0.370 ± 0.004	0.328 ± 0.004
$L_1 / (L_1 + L_2)$ (V)	0.584 ± 0.007	0.619 ± 0.005	0.654 ± 0.007	0.685 ± 0.007
$L_1 / (L_1 + L_2)$ (g')	0.573 ± 0.007	0.605 ± 0.005	0.645 ± 0.007	0.677 ± 0.008
$L_1 / (L_1 + L_2)$ (r')	0.595 ± 0.007	0.628 ± 0.005	0.662 ± 0.007	0.692 ± 0.007
$L_1 / (L_1 + L_2)$ (i')	0.604 ± 0.007	0.637 ± 0.004	0.670 ± 0.007	0.697 ± 0.007
r_1 side	0.4451 ± 0.0008	0.4701 ± 0.0006	0.4807 ± 0.0007	0.4949 ± 0.0010
r_2 side	0.3392 ± 0.0050	0.3068 ± 0.0024	0.2966 ± 0.0039	0.2819 ± 0.0052
Spot Parameters				
Spot 1	*$Star_1$*	*$Star_1$*	*$Star_1$*	*$Star_1$*
Colatitude (°)	51 ± 13	128 ± 21	51 ± 16	67 ± 19
Longitude (°)	102 ± 2	244 ± 2	260 ± 3	264 ± 2
Spot radius (°)	17 ± 4	15 ± 5	22 ± 5	17 ± 5
Temp. factor	0.83 ± 0.05	0.85 ± 0.09	0.83 ± 0.04	0.88 ± 0.06
Spot 2	—	*$Star_1$*	*$Star_1$*	*$Star_1$*
Colatitude (°)	—	108 ± 1	100 ± 15	70 ± 8
Longitude (°)	—	9 ± 1	336 ± 4	33 ± 7
Spot radius (°)	—	10 ± 1	10 ± 2	10 ± 3
Temp. factor	—	1.18 ± 0.03	0.83 ± 0.05	1.11 ± 0.06

[1]*Assumed.*
The subscripts 1 and 2 refer to the star being eclipsed at secondary and primary minimum, respectively.
Note: The errors in the stellar parameters result from the least-squares fit to the model. The actual uncertainties are considerably larger.

Table 9. Provisional absolute parameters.

Parameter	*Symbol*	*CD Sex*	*V365 Sge*	*V1148 Her*	*NSVS 9027851*
Stellar mass	M_1 ($M_\odot$)	0.95 ± 0.10	1.25 ± 0.11	0.99 ± 0.10	1.23 ± 0.11
	M_2 ($M_\odot$)	0.48 ± 0.05	0.52 ± 0.05	0.37 ± 0.04	0.40 ± 0.04
Semi-major axis	a ($R_\odot$)	1.97 ± 0.05	2.61 ± 0.05	2.00 ± 0.05	2.52 ± 0.05
Mean stellar radius	R_1 ($R_\odot$)	0.89 ± 0.02	1.23 ± 0.03	0.94 ± 0.02	1.24 ± 0.03
	R_2 ($R_\odot$)	0.66 ± 0.02	0.84 ± 0.02	0.60 ± 0.02	0.76 ± 0.02
Bolometric magnitude	$M_{bol,1}$	5.75 ± 0.09	4.4 ± 0.2	5.39 ± 0.08	4.47 ± 0.09
	$M_{bol,2}$	6.21 ± 0.12	5.0 ± 0.3	6.17 ± 0.10	5.35 ± 0.11
Stellar luminosity	L_1 ($L_\odot$)	0.40 ± 0.03	1.3 ± 0.3	0.56 ± 0.04	1.30 ± 0.10
	L_2 ($L_\odot$)	0.26 ± 0.03	0.8 ± 0.2	0.27 ± 0.03	0.58 ± 0.06
Surface gravity	log g_1 (cgs)	4.51 ± 0.05	4.35 ± 0.04	4.46 ± 0.05	4.34 ± 0.04
	log g_2 (cgs)	4.48 ± 0.05	4.31 ± 0.04	4.42 ± 0.05	4.28 ± 0.04

Note: The calculated values in this table are provisional. Radial velocity observations are necessary for direct determination of M1, M2 and a.

Table 10. Parameters of the V365 Sge tertiary component.

Parameter	*Value*	*Units*
P_3	12.032 ± 0.009	years
A_3	0.001887 ± 0.000002	days
e	*0.0	
$a_{12} \sin i_3$	0.3267 ± 0.0003	AU
f(m)	0.0002408 ± 0.0000008	$M_\odot$
M_3 ($i_3 = 90°$)	0.094 ± 0.004	$M_\odot$
M_3 ($i_3 = 60°$)	0.109 ± 0.005	$M_\odot$
M_3 ($i_3 = 30°$)	0.194 ± 0.011	$M_\odot$
a_3 ($i_3 = 90°$)	6.13 ± 0.14	AU
a_3 ($i_3 = 60°$)	6.09 ± 0.14	AU
a_3 ($i_3 = 30°$)	5.92 ± 0.13	AU

**Assumed*

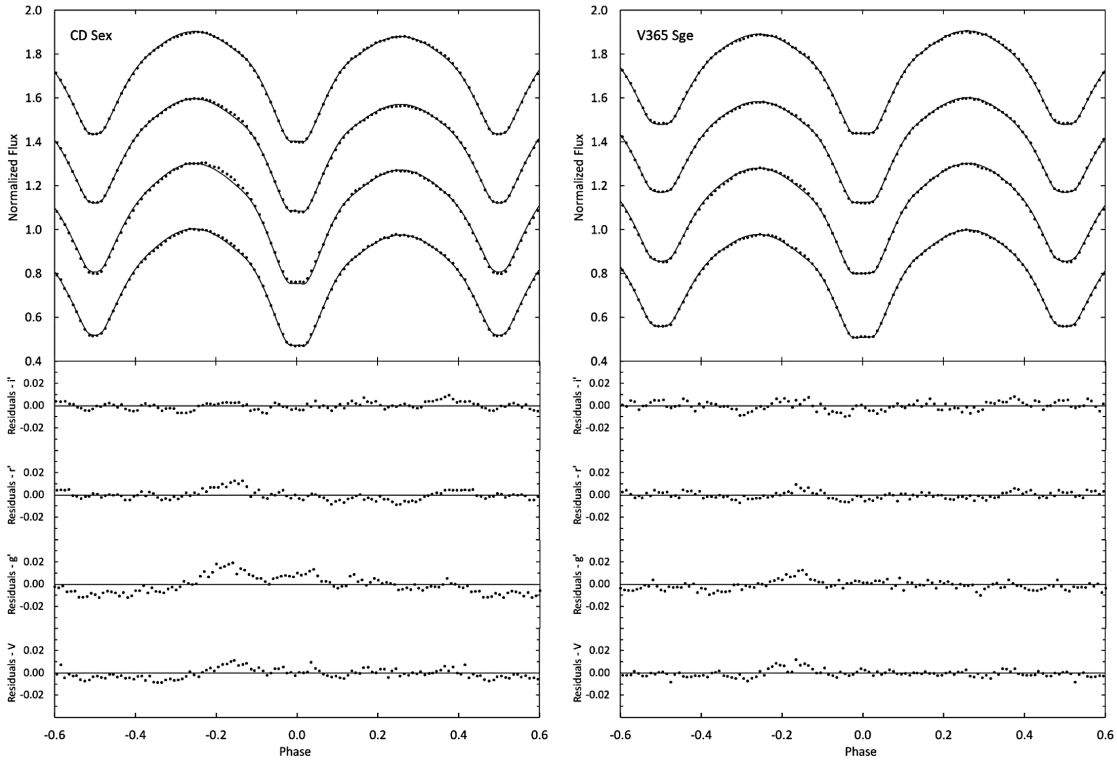

Figure 6. Comparison between the WD model fits (solid curve) and the observed normalized flux curves for CD Sex and V365 Sge. From top to bottom the passbands are i', r', g', and V. Each curve is offset by 0.3 for this combined plot. The residuals for the best-fit model are shown in the bottom panel. Error bars are omitted from the points for clarity.

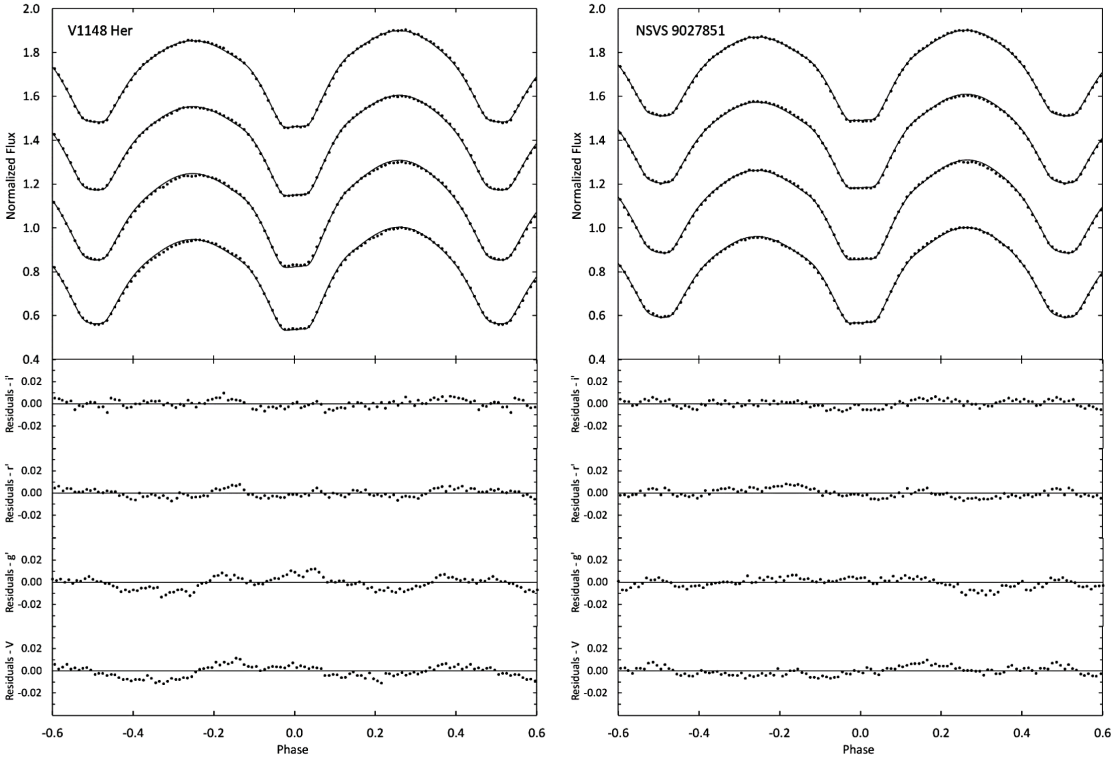

Figure 7. Comparison between the WD model fits (solid curve) and the observed normalized flux curves for V1148 Her and NSVS 9027851. From top to bottom the passbands are i', r', g', and V. Each curve is offset by 0.3 for this combined plot. The residuals for the best-fit model are shown in the bottom panel. Error bars are omitted from the points for clarity.

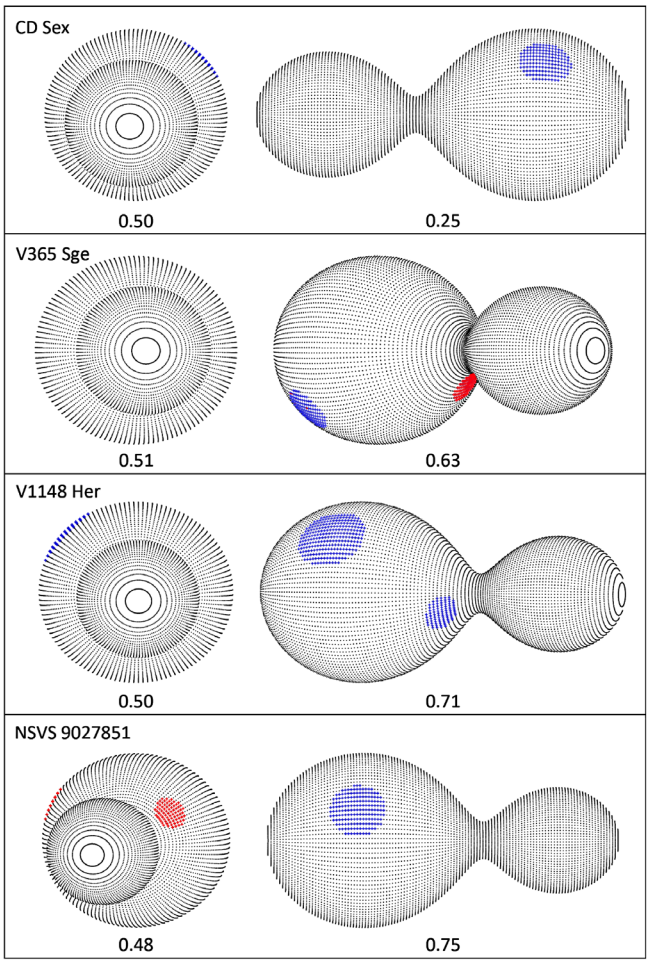

Figure 8. Roche Lobe surfaces of the best-fit WD spot model showing spot locations. The orbital phase is shown below each diagram.

Eclipse minima timings covering another cycle or two (12–24 years) will be necessary to confirm this tertiary star and revise the orbital parameters.

5. Conclusions

New high cadence multi-band photometric observations resulted in precision light curves and new minima timings for each star in this study. Light curve modeling with the WD program found a contact configuration for each system with the stars overfilling their critical Roche lobe. The solution mass ratios (q) should be well determined, given the light curves displayed total eclipses. Spot modeling was required to fit the light curve asymmetries, indicating magnetically active stars. The linear ephemerides of each system were updated using all available minima timings. The large mass differences and nearly equal temperatures of each system's component stars indicates a significant energy exchange between the stars.

The CD Sextantis system is a short period (P = 0.2688 d) contact binary. The orbital period of its K stars appears constant, though this conclusion is not certain given the large gaps in the few minima timings currently available (see Figure 3). The photometric solution gives an inclination of i = 87.7°, and a temperature difference of 233 K between the component stars. This system has a fill-out of 15% and its mass ratio, q = 0.502, is at the high end of the range when compared to the majority of observed totally eclipsing systems (Latković *et al.* 2021). The O'Connell (1951) effect is evident in the light curves, with Max II 0.026 magnitude brighter than Max I in the V passband. A single cool spot was modeled on the larger primary star to address this asymmetry. There is a small difference between the solution derived distance, 322 ± 12 pc, and the Gaia-DR3 distance of 288 ± 2 pc. This indicates the system's total luminosity is possibly overestimated in the model.

V365 Sagittae is a W-type contact binary that exceeds its critical lobe with a fill-out of 20%. This system has a mass ratio of q = 0.415, a temperature difference of 382 K between its component stars, and an orbital inclination nearly perpendicular to the sky (i = 89.1°). The light curves show Max I is brighter than Max II by 0.028 magnitude in the V passband. Minimizing the light curve asymmetries required the addition of both a hot and a cool star spot to the WD model. Both spots were located on the larger and cooler primary star. The solution derived distance, d = 520 ± 48 pc, when compared to the Gaia value, d = 471 ± 4 pc, is within the margin of errors. The period analysis of this system indicates the orbital period of the binary is slowly decreasing at a rate of $-1.055(2) \times 10^{-7}$ d · yr^{-1} and that there is a possible low mass tertiary component with a 12-year orbital period.

The photometric solution of V1148 Herculis gives an inclination of i = 88° and indicates an overcontact configuration with a fill-out of 20%. The component stars have a mass ratio of q = 0.370 and a temperature difference of 242 K. The larger cooler primary star has a spectral type of K1 and G9 for the smaller secondary star. The O'Connell effect is very apparent in the light curves, with Max I brighter than Max II by 0.061 magnitude in the V passband. The light curve asymmetries were modeled by adding two cool spots to the primary star. The derived system distance and the Gaia value are in good agreement, d = 288 ± 10 pc and d = 288 ± 1 pc, respectively. The period analysis, using the few minima times available, indicates a possible slowly decreasing orbital period.

NSVS 9027851 is a contact binary whose G stars orbit each other in 0.3627 day. There are too few minima times available to assess whether the orbital period is constant. The WD solution gives a fill-out of 22%, a mass ratio of q = 0.328, and a temperature difference of 246 K between its component stars. The O'Connell effect is quite noticeable in the light curves, with Max I 0.047 magnitude brighter than Max II in the V passband. A good fit between the observed and synthetic light curves was obtained by modeling both a cool and a hot spot on the primary star. The derived system distance is in good agreement with the Gaia value, d = 450 ± 16 pc and d = 430 ± 4 pc, respectively.

6. Acknowledgements

This research was made possible through the use of the AAVSO Photometric All-Sky Survey (APASS), funded by the Robert Martin Ayers Sciences Fund. This research has made use of the SIMBAD database and the VizieR catalogue access tool, operated at CDS, Strasbourg, France. This work has made use of data from the European Space Agency (ESA)

mission Gaia (https://www.cosmos.esa.int/gaia), processed by the Gaia Data Processing and Analysis Consortium (DPAC, https://www.cosmos.esa.int/web/gaia/dpac/consortium). Funding for the DPAC has been provided by national institutions, in particular the institutions participating in the Gaia Multilateral Agreement. Data from the Guo Shou Jing Telescope (the Large Sky Area Multi-Object Fiber Spectroscopic Telescope, LAMOST) were also used in this study. This telescope is a National Major Scientific Project built by the Chinese Academy of Sciences. Funding for the project has been provided by the National Development and Reform Commission. LAMOST is operated and managed by National Astronomical Observatories, Chinese Academy of Sciences. The author greatly appreciated the comments and suggestions of the anonymous referee.

References

Bradstreet, D. H., and Steelman, D. P. 2002, *Bull. Amer. Astron. Soc.*, **34**, 1224.
Diethelm, R. 2003, *Inf. Bull. Var. Stars*, No. 5438, 1.
Diethelm, R. 2004, *Inf. Bull. Var. Stars*, No. 5543, 1.
Diethelm, R. 2010, *Inf. Bull. Var. Stars*, No. 5945, 1.
Diethelm, R. 2011, *Inf. Bull. Var. Stars*, No. 5992, 1.
Diethelm, R. 2012a, *Inf. Bull. Var. Stars*, No. 6011, 1.
Diethelm, R. 2012b, *Inf. Bull. Var. Stars*, No. 6029, 1.
Drake, A. J., *et al.* 2014, *Astrophys. J., Suppl. Ser.*, **213**, 9.
Eker, Z., *et al.* 2020, *Mon. Not. Roy. Astron. Soc.*, **496**, 3887.
Gaia Collaboration. 2022, VizieR Online Data Catalog: Gaia DR3 Part 1, I/355 (*Astron. Astrophys.*, in prep.).
Gettel, S. J., Geske, M. T., and McKay, T. A. 2006, *Astron. J.*, **131**, 621.
Green, G. M., Schlafly, E., Zucker, C., Speagle, J. S., and Finkbeiner, D. 2019, *Astrophys. J.*, **887**, 93.
Hambálek, Ľ., and Pribulla, T. 2013, *Contrib. Astron. Obs. Skalnaté Pleso*, **43**, 27.
Henden, A. A., *et al.* 2015, AAVSO Photometric All-Sky Survey, data release 9 (https://www.aavso.org/apass).
Hoffman, D. I., Harrison, T. E., and McNamara, B. J. 2009, *Astron. J.*, **138**, 466.
Hübscher, J. 2011, *Inf. Bull. Var. Stars*, No. 5984, 1.
Hübscher, J. 2014, *Inf. Bull. Var. Stars*, No. 6118, 1.
Hübscher, J. 2016, *Inf. Bull. Var. Stars*, No. 6157, 1.
Hübscher, J., and Lehmann, P. B. 2013, *Inf. Bull. Var. Stars*, No. 6070, 1.
Hübscher, J., and Monninger, G. 2011, *Inf. Bull. Var. Stars*, No. 5959, 1.
Hubscher, J., Lehmann, P. B., Monninger, G., Steinbach, H.-M., and Walter, F. 2010, *Inf. Bull. Var. Stars*, No. 5941, 1.
Jayasinghe, T., *et al.* 2018, *Mon. Not. Roy. Astron. Soc.*, **477**, 3145.
Jester, S., *et al.* 2005, *Astron. J.*, **130**, 873.
Kafka, S. 2017, variable star observations from the AAVSO International Database (https://www.aavso.org/aavso-international-database).
Khruslov, A. V. 2006, *Perem. Zvezdy Prilozh.*, **6**, 16 (http://www.astronet.ru/db/varstars/msg/eid/PZP-06-0016).
Kurucz, R. L. 2002, *Baltic Astron.*, **11**, 101.
Kwee, K. K., and van Woerden, H. 1956, *Bull. Astron. Inst. Netherlands*, **12**, 327.
Latković, O., Čeki, A., and Lazarević, S. 2021, *Astrophys. J., Suppl. Ser.*, **254**, 10.
Liao, W.-P., and Qian, S.-B. 2010, *Mon. Not. R. Astron. Soc.*, **405**, 1930.
Locher, K. 2005, *Open Eur. J. Var. Stars*, **3**, 1 (http://var.astro.cz/oejv/oejv.php?oejv=3).
Lucy, L. B. 1968, *Astrophys. J.*, **151**, 1123.
Lucy, L. B., and Wilson, R. E. 1979, *Astrophys. J.*, **231**, 502.
Masaryk University, Brno. 2022, SuperWASP Wide Angle Search for Planets database (https://wasp.cerit-sc.cz/form).
Mirametrics. 2015, Image Processing, Visualization, Data Analysis, (https://www.mirametrics.com).
O'Connell, D. J. K. 1951, *Publ. Riverview Coll. Obs.*, **2**, 85.
Pecaut, M. J., and Mamajek, E. E. 2013, *Astrophys. J., Suppl. Ser.*, **208**, 9.[1]
Pojmański, G. 2002, *Acta Astron.*, **52**, 397.
Pribulla, T., and Rucinski, S. M. 2006, *Astron. J.*, **131**, 2986.
Qian, S.-B., Liu, N.-P., Liao, W.-P., He, J.-J., Liu, L., Zhu, L.-Y., Wang, J.-J., and Zhao, E.-G. 2013, *Astron. J.*, **146**, 38.
Richards, J. W., Starr, D. L., Miller, A. A., Bloom, J. S., Butler, N. R., Brink, H., and Crellin-Quick, A. 2012, *Astrophys. J., Suppl. Ser.*, **203**, 32.
Richmond, M. W. 2002, *Inf. Bull. Var. Stars*, No. 5221, 1.
Ruciński, S. M. 1969, *Acta Astron.*, **19**, 245.
Shappee, B. J., *et al.* 2014, *Astrophys. J.*, **788**, 48 (ASAS-SN Catalog of Variable Stars: II, https://asas-sn.osu.edu/).
Terrell, D. 2022, *Galaxies*, **10**, 8.
Terrell, D., and Wilson, R. E., 2005, *Astrophys. Space Sci.*, **296**, 221.
Terrell, D., Gross, J., and Cooney, W. R. 2012, *Astron. J.*, **143**, 99.
Tonry, J., *et al.* 2018, *Astrophys, J.*, **867**, 105.
van Hamme, W. 1993, *Astron. J.*, **106**, 2096.
van Hamme, W., and Wilson, R. E. 1998, *Bull. Amer. Astron. Soc.*, **30**, 1402.
Watson, C., Henden, A. A., and Price, C. A. 2014, AAVSO International Variable Star Index VSX (Watson+, 2006–2014; https://www.aavso.org/vsx).
Willmer, C. N. A. 2018, *Astrophys. J., Suppl. Ser.*, **236**, 47.
Wilson, R. E., 1978, *Astrophys. J.*, **224**, 885.
Wilson, R. E., and Biermann, P. 1976, *Astron. Astrophys.*, **48**, 349.
Wilson, R. E., and Devinney, E. J. 1971, *Astrophys. J.*, **166**, 605.
Woźniak, P. R., *et al.* 2004, *Astron. J.*, **127**, 2436.

[1]Pecaut, M. J., and Mamajek, E. E. (2013): http://www.pas.rochester.edu/~emamajek/EEM_dwarf_UBVIJHK_colors_Teff.txt